

# Combined Impacts of ENSO and MJO on the 2015 Growing Season Drought on the Canadian Prairies

Zhenhua Li<sup>1,2</sup>, Yanping Li<sup>1</sup>, Barrie Bonsal<sup>3</sup>, Alan H. Manson<sup>2</sup>, Lucia Scaff<sup>1</sup>

<sup>1</sup>Global Institute for Water Security, University of Saskatchewan, Saskatoon, Saskatchewan, Canada S7N3H5

<sup>2</sup>Institute of Space and Atmospheric Studies, University of Saskatchewan, Saskatoon, Saskatchewan, Canada

<sup>3</sup>National Hydrology Research Center, Environment and Climate Change Canada, Saskatoon, SK, Canada

*Correspondence to:* Dr. Yanping Li (yanping.li@usask.ca); Dr. Zhenhua Li (zhenhua.li@usask.ca)

## Abstract

Warm-season precipitation on the Canadian Prairies plays a crucial role in agricultural production. This research investigates how the early summer 2015 drought across the Canadian Prairies is related to tropical Pacific forcing. The significant deficit of precipitation in May and June of 2015 coincided with a warm phase of El Nino-Southern Oscillation (ENSO) and a negative phase of Madden-Julian Oscillation (MJO)-4 index, which favour a positive geopotential height anomaly in western Canada. Our further investigation during the instrumental record (1979-2016) shows that warm-season precipitation in the Canadian Prairies and the corresponding atmospheric circulation anomalies over western Canada teleconnected with the lower boundary conditions in the tropical western Pacific. Our results indicate that MJO can play a crucial role in determining the summer precipitation anomaly in the western Canadian Prairies when the equatorial central Pacific is warmer than normal ( $\text{NINO4} > 0$ ) and MJO is more active. This teleconnection is due to the propagation of a stationary Rossby wave that is generated in the MJO-4 index region. When the tropical convection around MJO-4 index region (western tropical Pacific, centered over 140°E) is more active than normal ( $\text{NINO4} > 0$ ), a Rossby wave train originates from western Pacific and propagates into midlatitude over North America causing a persistent anomalous ridge in the upper level over western Canada, which favours dry conditions over the region.

## 1 Introduction

The Canadian Prairies depends on summer precipitation especially during the early to mid-growing season (May through August) when the majority of annual precipitation normally occurs (e.g., Bonsal *et al.* 1993). High natural variability in growing season precipitation causes periodic occurrences

26 of extreme precipitation (Li *et al.* 2017; Liu *et al.* 2016 and droughts that are often associated with  
27 reduced agriculture yields, low streamflow, and increased occurrence of forest fires (Wheaton *et al.*  
28 2005, Bonsal and Regier 2007). Drought events with great environmental and economic impacts have  
29 occurred in 1961, 1988, 2001-2002, and as recent as 2015 (Dey 1982, Liu *et al.* 2004, Bonsal *et al.*  
30 1999, Wheaton *et al.* 2005, Shabbar *et al.* 2011, Bonsal *et al.* 2013, Szeto *et al.* 2016). The sub-seasonal  
31 forecast of precipitation for the growing season is crucial for the agriculture, water resource  
32 management, and the economy of the region. Therefore, an investigation into the causes of inter-annual  
33 variability in the growing season precipitation of the Canadian Prairie is needed.

34 Low precipitation and extended dry periods on the Canadian Prairies are often associated with an  
35 upper-level ridge and a persistent high pressure centered over the region (Dey 1982, Liu *et al.* 2004).  
36 These prolonged atmospheric anomalies often concurred with abnormal boundary layer conditions such  
37 as a large-scale sea surface temperature (SST) anomalies in the Pacific Ocean (Shabbar and Skinner  
38 2004). Large scale oscillation in the SST anomalies in the Pacific Ocean, namely El Nino, and the  
39 Pacific Decadal Oscillation (PDO), can affect the hydroclimatic pattern in summer over North America,  
40 although the strongest impacts of these boundary conditions occur during the boreal winter. Inter-annual  
41 variability such as El Nino-Southern Oscillation (ENSO) is linked with extended droughts in the Prairies  
42 (Bonsal *et al.* 1999, Shabbar and Skinner 2004). Interdecadal oscillations such as the PDO, and the  
43 Atlantic Multi-decadal Oscillation (AMO) also affect the seasonal temperature and precipitation in the  
44 Canadian Prairies (Shabbar *et al.* 2011).

45 ENSO's relationship with Canadian Prairie precipitation has been studied extensively. The warm  
46 phase of ENSO often favours drought in this region, especially during the growing season after the  
47 mature phase of El Nino with the North Pacific Mode (NPM, Hartmann *et al.* 2015) positive like North  
48 Pacific SST anomaly pattern (Bonsal and Lawford 1999, Shabbar and Skinner 2004). Previous  
49 investigations (e.g., Shabbar *et al.* (2011)) have found that El Nino events are associated with a summer

50 moisture deficit in western Canada while La Nina events cause an abundance of moisture in far western  
51 Canada (British Columbia and Yukon). However, they also noted that although tropical SST variability  
52 accounted for some aspects of the large-scale circulation anomalies that influence Canadian Prairies  
53 meteorological drought, a consistent and clear-cut relationship was not found. North Pacific SST warm  
54 anomalies, which often follow a matured El Nino, and accompanying atmospheric ridging leads to  
55 extended dry spells over the Prairies during the growing season (Bonsal and Lawford 1999).  
56 Furthermore, in association with the recent North Pacific SST anomaly from 2013 to 2014, researchers  
57 have attributed the precipitation deficit in California during 2013 to the anomalous upper-level ridge  
58 over the western North America (Wang *et al.* 2014, Szeto *et al.* 2016).

59 The aforementioned SST variations, mostly vary on inter-annual and decadal scales. Another  
60 important factor that affects the weather patterns in North America is the Madden-Julian Oscillation  
61 (MJO), an intra-seasonal (40-90 days) oscillation in convection and precipitation pattern over the  
62 Tropics (Madden and Julian 1971, Zhang 2005, Riddle *et al.* 2013, Carbone and Li 2015). MJO is a  
63 coupled atmosphere-ocean oscillation involving convection and large-scale equatorial waves, which  
64 produces an eastward propagation of tropical convection anomaly (Madden and Julian 1971). The MJO  
65 affects the winter temperature and precipitation in North America and Europe through its impact on  
66 moisture transport associated with the “Pineapple Express” and its effects on the North Atlantic  
67 Oscillation and stratospheric polar vortex (Cassou 2008, Garfinkel *et al.* 2012, Rodney *et al.* 2013).  
68 MJO is also connected to the summer precipitation anomalies in the Southwest United States (Lorenz  
69 and Hartmann 2006). During warm season, MJO's impact on Canadian Prairie precipitation has not been  
70 thoroughly investigated as MJO's amplitude is weak during spring and early summer. The amplitude of  
71 MJO in spring and early summer is related to the inter-annual variation of tropical SST, especially the  
72 SST in central Pacific (Hendon *et al.* 2007, Marshall *et al.* 2016). MJO in terms of the Real-time  
73 Multivariate MJO index (RMM, Wheeler and Hendon 2004), was extremely strong in the early spring of

74 2015 with a positive PDO-like SST anomaly in the central Pacific and at the same time, El Nino started  
75 to strengthen.

76 MJO activities in the western Pacific under the modulation of inter-annual SST variability have  
77 the potential to act together with ENSO and impact mid-tropospheric circulation over western Canada  
78 and thus, warm season precipitation over the Canadian Prairies. The goal of this study is to demonstrate  
79 that MJO have contributed to the 2015 growing season drought in the Canadian Prairies through the  
80 propagation of stationary Rossby wave. Subsequently, further investigations are carried out to determine  
81 if similar relationships exist in association with other summer extreme precipitation events during  
82 instrumental record (1979-2016). Section 2 provides the datasets and methodology used in this paper  
83 while section 3 presents the analysis of the upper-level circulation anomaly and SST pattern associated  
84 with the 2015 drought. This is followed by the examination of the effects of central Pacific SST  
85 anomalies and MJO on the summer precipitation in the Canadian Prairies. The mechanism by which  
86 MJO affects summer precipitation when equatorial central Pacific SST is warmer than normal is  
87 discussed in section 4 followed by a summary and concluding remarks in section 5.

## 88 **2 Data and Methodology**

89 Multiple observation and reanalysis datasets are used to investigate the circulation anomalies  
90 associated with Canadian Prairie growing season (May-August) precipitation. Observed precipitation is  
91 taken from the Climate Prediction Center (CPC) Merged Analysis of Precipitation (CMAP) dataset (Xie  
92 and Arkin 1997). Geopotential height fields from the National Center for Environmental Predictions  
93 (NCEP) Reanalysis (Kalnay *et al.* 1996) and the European Center for Medium-Range Weather Forecast  
94 (ECMWF)'s ERA Interim reanalysis (Dee *et al.* 2011) are used to analyze the mid- and upper-level (200  
95 hPa and 500 hPa) atmospheric circulation patterns.

96 To represent the central Pacific SST anomaly, NINO4 SST index (Rayner *et al.* 2003) from CPC

97 of National Oceanic and Atmospheric Administration (NOAA) is used since the NINO4 region is near  
98 the central Pacific and spans over the dateline (5°S-5°N, 160°E-150°W). Multivariate ENSO Index  
99 (MEI) data are retrieved from NOAA's Climate Data Center (CDC) website and is used to determine the  
100 ENSO phase (Wolter 1987, Wolter and Timlin 1993). In particular, El Nino condition is defined when  
101 the monthly mean index of MEI is larger than 0.5 (Andrews *et al.* 2004).

102 The Real-time Multivariate MJO series (RMM1 and RMM2) developed by Wheeler and Hendon

103 (2004) are used to identify periods of strong MJO activity as the MJO amplitudes are directly calculated  
104 by the square root of RMM1 + RMM2. For MJO intensities, we used the monthly averaged pentad MJO  
105 indices from NOAA CPC's MJO index (Xue *et al.* 2002), which have 10 indices representing locations  
106 around the globe. The CPC's MJO index is based on Extended Empirical Orthogonal Function (EEOF)  
107 analysis on pentad velocity potential at 200 hPa. Ten MJO indices on a daily scale are constructed by  
108 projecting the daily (00Z) velocity potential anomalies at 200 hPa (CHI200) onto the ten time-lagged  
109 patterns of the first EEOF of pentad CHI200 anomalies (Xue *et al.* 2002). Negative values of ten MJO  
110 indices correspond to enhanced convection in the 10 regions centered on 20°E, 70°E, 80°E, 100°E,  
111 120°E, 140°E, 160°E, 120°W, 40°W and 10°W in the tropics. MJO indices usually vary between -2 to 2  
112 with negative values indicating above average convective activities in the corresponding region.

113 Because boreal summer usually corresponds to a period of weaker amplitude of MJO than the winter,  
114 we chose the monthly mean value of -0.3 as the criterion of strong convection which is connected to  
115 MJO as the index generally vary between -1 and 1. An MJO-4 index (centered on 140°E) of less than -  
116 0.3 was considered a relatively strong convection in the western Pacific, which has been found to be a  
117 source region of stationary Rossby waves (Simmons 1980). SST observations include Extended  
118 Reconstructed Sea Surface Temperature (ERSST) v4 (Huang *et al.* 2015). Outward Longwave Radiation  
119 (OLR) data from NOAA Interpolated Outgoing Longwave Radiation are used to derived the composite  
120 of anomalies of OLR for a certain phase of MJO.

121 Our study focuses on growing season precipitation in the provinces of Alberta and Saskatchewan  
122 in the Canadian Prairies, where the largest deficits were observed in 2015. Specifically, the regional  
123 mean precipitation over 115°-102.5°W, 50°-57.5°N is used (boxed area in Fig. 1, top panel) to represent  
124 the Canadian Prairies east of the Rocky Mountains and south of the boreal forest. The region chosen  
125 also covers most of the arable land in the Canadian Prairies. Considering the unique MJO-4 and NINO4  
126 indices for 2015, the relationship between the Prairies' warm season (May-August) precipitation with  
127 MJO-4 and ENSO during the instrumental records are investigated using correlation and regression.  
128 Though the dry months of the 2015 growing season are May and June when MJO-4 was in negative  
129 phase, we want to study the statistical relationship between MJO-4 and the Prairies' precipitation in  
130 growing season (May-August). The possible mechanism behind the correlation between MJO-4 and the  
131 Prairie's warm season precipitation during El Nino condition is further investigated by analyzing the  
132 upper-level circulation associated with convection in the tropical Pacific and stationary Rossby waves in  
133 mid-latitudes.

134

### 135 **3 Results**

#### 136 **3.1 The 2015 Summer Drought**

137 Almost all of western Canada including British Columbia, the southern Northwest Territories,  
138 Alberta and Saskatchewan had negative precipitation anomalies during May and June 2015. The top plot  
139 in Fig. 1 shows the precipitation anomaly in percentage relative to the climatology (1981-2010 long  
140 term mean) in Canada during May and June 2015. The bottom plot in Fig. 1 presents the monthly  
141 precipitation anomaly averaged over the region encompassed by the dash lines (top panel in Fig. 1). The  
142 average annual cycle of the regional precipitation has a dry period between February and May and June

143 has the largest precipitation in all months. The May and June 2015 precipitation deficit was also  
144 accompanied by a relatively dry period from February to April [Szeto *et al.* 2016], which added to the  
145 drought conditions.

146 Fig. 1 Top: Precipitation anomalies (mm) from CMAP over the region (115°W-102.5°W, 50°N-57.5°N) during May  
147 and June 2015. Bottom: time series of monthly precipitation anomaly over boxed region between September 2013 and  
148 August 2015.

149 The mid- and upper-level geopotential height (GPH) anomaly averaged in May and June are  
150 examined together with SST anomaly and ENSO, MJO-4 indices for 2014 and 2015. The 500 hPa GPH  
151 anomaly for May and June 2015 shows strong positive anomalies near Alaska and the British Columbia  
152 coast (Fig. 2), which is consistent with the findings for other episodes of growing season droughts (e.g.,  
153 Dey 1982; Bonsal and Wheaton, 2005). Accompanying this anomalous ridge, are above normal SSTs in  
154 the northeast Pacific off the coast of North America and the central-eastern Pacific (Fig. 3). Both ENSO  
155 and the NPM are in positive phases that corresponds to a warmer SST near the Pacific coast of North  
156 America, consistent with the positive GPH anomalies in western Canada and Alaska. The ridge in  
157 Alaska/Bering Straits and the one near British Columbia coast have been previously associated with El  
158 Nino and North Pacific SST anomaly such as NPM (Shabbar *et al.* 2011). The monthly mean anomalous  
159 ridge prevents storms from reaching the British Columbia coast and the Canadian Prairies causing  
160 extended dry spells. Therefore, the GPH anomaly in early growing season in 2015 is consistent with the  
161 precipitation anomaly in these regions. The anomalous upper-level ridge in the Western United States  
162 and Canada in 2014 and 2015 have also been associated with the developing El Nino and the other main  
163 components of Pacific SST variation such as NPM by several recent studies (Hartmann *et al.* 2015, Lee  
164 *et al.* 2015, Li *et al.* 2017).

165 Fig. 2 NCEP GPH anomaly at 500hPa during May and June 2015 when the precipitation deficit was the largest.

166 The average SST anomaly during the growing season (May-June, July-August) of 2015. shows a  
167 persistent strong positive anomaly in the northeast and eastern equatorial Pacific (Fig. 3), which  
168 corresponds to the warm phase of NPM and ENSO. SSTs in the eastern tropical Pacific warmed  
169 increasingly since the end of 2014 and qualified as an El Nino in early 2015. The NPM became positive  
170 in the fall 2013, turned exceptionally strong in 2014 and persisted to 2015 (Hartmann 2015). The  
171 anomalous ridge is concurrent with strong SST anomalies in the tropical Pacific and extratropical North  
172 Pacific. NPM, as the third EOF of Pacific SST (30°S-65°N), has also a strong connection to the  
173 anomalous ridge in western North America and trough in the eastern US and Canada in 2013-2014  
174 winter (Hartmann 2015, Lee *et al.* 2015). During the ENSO-neutral condition in 2013 and 2014, the  
175 precursor of ENSO, so-called "footprinting" mechanism is considered to cause this anomalous ridge in  
176 western North America (Wang *et al.* 2014).

177 The variation of Canadian Prairies' precipitation and its relationship with SST modes and MJOs  
178 are shown in Fig. 4. The time series of monthly RMM amplitude, NINO4 index, MJO-4 indices and the  
179 Canadian Prairies precipitation anomaly from January 2014 to December 2015 shows the atmospheric-  
180 oceanic circulation indices for the drought in 2015. In May and June 2015, the western Pacific  
181 witnessed a strong MJO-4 negative index, whereas in July the MJO-4 index became positive. This  
182 corresponds well with the precipitation anomaly in Fig. 1. As shown in Fig. 3, El Nino continued to  
183 strengthen in July and August 2015; while at the same time the MJO-4 index increased. The increase of  
184 the MJO-4 index corresponded to the active convection associated with MJO that moved away from the  
185 tropical western Pacific region and propagated eastward into the central Pacific. Coincident with this  
186 change in MJO, the precipitation in the Canadian Prairies then returned to slightly above normal in July.

187 The good correspondence of MJO-4 and the negative precipitation anomaly suggests a link  
188 between MJO and Prairie precipitation during growing season. Although El Nino and associated  
189 Northeast Pacific SST warm anomaly (i.e., NPM) in summer 2015 can be a contributing factor for the

190 persistent upper-level ridge over the west coast of Canada, it cannot fully explain the drought condition  
191 in west Canada, as these SSTs do not guarantee a prolonged dry spell as shown by correlation analysis  
192 (Table 1). The negative MJO-4 index concurred with the negative anomaly of Prairie precipitation in  
193 2015, which prompts the investigation of their relationship with the instrumental records.

194 Fig. 3 The mean SST anomaly (°C) from ERSST v4 in May-August 2015.

195 Fig. 4 RMM amplitude anomaly, NINO4, MJO 4 indices and precipitation anomaly of Canadian Prairies from January 2014  
196 to Dec 2015.

197

## 198 **3.2 Instrumental record**

199 El Nino and its associated North Pacific SST anomaly may contribute to extended dry spells in  
200 Canadian Prairies after the mature phase of El Nino (Bonsal *et al.* 1993) on an inter-annual time scale.  
201 ENSO, however, is not a strong intra-seasonal to seasonal predictor of Canadian Prairie summer  
202 precipitation. The lack of strong correlation between the Prairies' precipitation and ENSO index can be  
203 caused by many factors that affect the Prairies' precipitation on a seasonal and sub-seasonal scale.  
204 Shabbar and Skinner (2004) showed the connection between the warm phase of ENSO and western  
205 Canadian drought through singular value decomposition analysis. However, they also found other  
206 modes of SST variation (e.g., positive phase of PDO) can produce wet condition in the Prairies. Here we  
207 present a new result showing that under warm central Pacific SST conditions ( $\text{NINO4} > 0$ ), a certain  
208 phase of MJO, which connected to the active convection in the tropical western Pacific (Li and Carbone  
209 2012), plays an important role in modulating the growing season precipitation in the Canadian Prairies.

210 Table 1 Correlation between mean precipitation anomaly in the Prairies from CMAP and MEI, MJO indices 4. MJO  
211 indices and CMAP are from 1979 to 2016.

212

213 The correlation coefficients between the mean regional precipitation anomaly over Canadian

214 Prairies and MJO-4 indices and MEI from May to August are shown in Table 1. The correlation

215 between MEI alone and the precipitation anomalies is not significant. The correlation between MJO-4

216 and precipitation in the Prairies is 0.18 with a p-value of 0.023, which indicates that stronger tropical

217 convection in the equatorial region centered around 140°E favours less precipitation in the Canadian

218 Prairies from May to August. When NINO4 is larger than 0, the correlation between MJO-4 and

219 growing season precipitation is 0.33 with a p-value of 0.0015. Conversely, the correlation between

220 MJO-4 and Canadian Prairie precipitation is -0.01 when  $NINO4 < 0$ .

221 Fig. 5 The scatter plot of monthly precipitation anomaly (mm/month) as a function of MJO-4 and NINO4. Each

222 asterisk represents a month from May to August 1979-2016. Circled asterisk denotes a month with precipitation anomaly larger

223 than 18 mm/month. The blue circles are months with positive precipitation anomaly and the red circles are months with negative

224 precipitation anomaly. The sizes of circles denote the magnitudes of the anomalies (large  $> 30$  mm/month, medium  $> 24$

225 mm/month, small  $> 18$  mm/month). The shaded area denotes  $NINO4 > 0$  and MJO-4 index  $< 0$ .

226 The scatter plot in Fig. 5 shows the distribution of monthly precipitation anomaly versus MJO-4

227 index and NINO4 index. Circled asterisk denotes a month with precipitation anomaly larger than 18

228 mm/month and the red (blue) circles denote a negative (positive) precipitation anomaly. The criterion

229 for precipitation anomaly to be emphasized by the circles is roughly one third of the mean monthly

230 precipitation in the growing season. The size of the circle represents the magnitude of the monthly

231 precipitation anomalies. The bottom-right region indicated by shading, under  $NINO4 > 0$  condition,

232 negative MJO-4 corresponds to a quadrant that have many more dry than wet months. We noticed that

233 some significant dry months are not in the shaded area, which corresponds to the dry months occurring

234 during La Nina or in the period after the mature phase of El Nino (Bonsal *et al.* 1999). Summer drought

235 in the Prairies can occur in both phases of ENSO or any other teleconnection indices. For example, for

236 the summer drought that happened in the Prairies from 1999 to 2005, the large-scale anomalous patterns

237 of SST first showed La Nina conditions and then became a weak El Nino in the latter half of the period

238 (Hanesiak *et al* 2011). Bonsal and Wheaton (2005) showed that the tropospheric atmospheric  
239 circulation patterns in 2001 and 2002 lacked the typical meridional flow in the North Pacific and North  
240 America during drought in western Canada. Their results show that the drought in 1999-2005 was  
241 related to the expansion of the continuous drought happened in the US to the north.

242 Fig. 6 The box-percentile plot of Canadian Prairies precipitation anomaly during growing season under different  
243 ENSO conditions.

244 The impact of ENSO on the growing season precipitaiton over Canadian Prairies is investigated.  
245 The box-percentile plot in Fig. 6 shows the distribution of monthly Canadian Prairies' precipitation  
246 anomalies from May to August along with different ENSO conditions. In general, under El Nino and  
247 neutral ENSO conditions, the precipitation anomalies are centered around 0, and there is no bias toward  
248 either end. Under La Nina condition, the mean precipitation has a positive bias. There are only 10  
249 summer months under La Nina condition, whereas there are 71 months under El Nino and neutral  
250 condition.

251 The distributions of precipitation anomalies versus MJO-4 index under different ENSO  
252 conditions are shown in Fig. 7. For  $\text{NINO4} > 0$ , the precipitation anomaly has a negative tendency when  
253  $\text{MJO-4} < -0.3$ . With  $\text{NINO4} < 0$ , there is no negative tendency for  $\text{MJO-4} < -0.3$ . Therefore, Fig. 6 and 7  
254 agrees with the significant correlation between precipitation and MJO-4 under  $\text{NINO4} > 0$ , relative to  
255 ENSO in Table 1.

256 Fig. 7 Box-percentile plots of Canadian Prairies' precipitation anomaly during growing season versus MJO-4 under  
257 warm NINO4 ( $\text{NINO4} > 0$ , left) and cold NINO4 ( $\text{NINO4} < 0$ , right) SST condition.

258 The correlation between MJO-4 and the Prairies' precipitation during growing season leads us to  
259 investigate the underlying circulation anomalies. Fig. 8 presents the regressed stream function and wind  
260 field at 200 hPa in the mid-latitudes (north of  $30^{\circ}\text{N}$ ) on the negative MJO-4 index from May to August  
261 under warm NINO4 SST condition ( $\text{NINO4} \geq 0$ ). In the tropics ( $10^{\circ}\text{S}$ - $20^{\circ}\text{N}$ ), during Northern

262 Hemisphere summer, the OLR, velocity potential and divergent wind vector are presented. Only  
263 regression patterns having p-values lower than 0.05 are plotted for OLR and velocity potential. The  
264 negative MJO-4 index corresponds to a negative anomaly in OLR, stronger convection and larger than  
265 average divergence in the region centered around 150°E. The strong convection anomaly centers around  
266 150°E, 5°N with divergent wind extending well into the subtropics in the Northern Hemisphere. The  
267 positive GPH/stream function anomaly extended from Japan to central Pacific is associated with the  
268 enhanced convection and divergence in the upper troposphere over the western tropical-subtropical  
269 Pacific. A Rossby wave train linked to the OLR anomaly and strong divergence in the western Pacific  
270 propagate eastward into North America. To better demonstrate the propagation of the wave train, we  
271 conducted a ray tracing of stationary Rossby wave following the nondivergent barotropic Rossby wave  
272 theory of Hoskins and Karoly (1981) and Hoskins and Ambrizzi (1993). Equation 1 describes the group

273 velocity, which represent the propagation of wave activity.  $C_{gx}$  and  $C_{gy}$  are the group velocity  
274 components on zonal and meridional directions;  $\bar{U}$  and  $\bar{V}$  are the mean zonal and meridional winds;  $q$  is  
275 the mean absolute vorticity;  $K$ ,  $k$ ,  $l$  are the total wave number, zonal wavenumber and meridional  
276 wavenumber, respectively. The ray path is integrated using a fourth-order Runge-Kutta method.

277

$$C_{gx} = \bar{U} + \frac{(k^2 - l^2)q_y - 2klq_x}{K^4}$$

279

Equation (1)

$$C_{gy} = \bar{V} + \frac{(k^2 - l^2)q_x + 2klq_y}{K^4}$$

280

281 Under average conditions in May-August derived from ERA-Interim at 200 hPa with NINO4 > 0.5 or  
282 NINO4 < -0.5, we released rays with a total wavenumber matching with the mean flow at the  
283 extratropical location of the OLR anomaly (140°E-150°E, 25°N-30°N). For quasi-stationary waves, the

284 wavenumber is determined by the basic zonal flow and background absolute vorticity gradient through  
285 the dispersion relation. For  $\text{NINO4} > 0.5$  May-August condition,  $K = 4.14$ . With this total wavenumber  
286 and launching angle from  $0\text{-}60^\circ$  relative to the zonal direction, Rossby wave rays (colored by red,  
287 orange to blue according to their angle from  $0^\circ$  to  $60^\circ$ ) released at  $140^\circ\text{W}$ ,  $20^\circ\text{N}$  can propagate  
288 successfully to the western Canada for those with smaller launching angles as shown the right in Fig. 9.  
289 With  $\text{NINO4} < -0.5$ , the zonal wind in the source region is weaker, and the meridional gradient of  
290 absolute vorticity is stronger due to its relative further southern position to the subtropical jet. The total  
291 wavenumber for stationary Rossby waves is 6.2, determined by the mean May-August condition for  
292  $\text{NINO4} < -0.5$ . The waves with shorter wavelength tend to be evanescent near the source region as  
293 shown in the left plot in Fig. 9. However, there is no significant difference in ray-path under  $\text{NINO4} < -0.5$   
294 condition compared to  $\text{NINO4} > 0.5$ , if the source wavenumbers are set to the same value (results  
295 not shown). The changes in the mean conditions from El Nino to La Nina are not sufficient to alter the  
296 propagation condition for Rossby waves.

297

## 298 **4 Discussion**

299 Summer of 2015 is the first summer after the developing of El Nino during 2014-2015 winter.  
300 Though the upper-level GPH pattern, seen in summer 2015, can be attributed to the SST modes in the  
301 Pacific, namely ENSO and NPM, the precipitation in the Western Canadian Prairie is not strongly  
302 correlated with either. Bonsal and Lawford (1999) found that more extended dry spells tend to occur in  
303 Canadian Prairies during the second summer following the mature stage of the El Nino events. The  
304 winter precipitation in Canada has a strong connection to ENSO (Shabbar *et al.* 1997), whereas summer  
305 precipitation, in most regions of western Canada (except the coast of British Columbia and Southern

306 Alberta), does not have a significant correlation with ENSO. This is consistent with our investigation  
307 using instrumental records from 1948 to 2016.

308 Growing season precipitation in the Canadian Prairies is affected by many factors, precipitation  
309 deficits can occur under various circulation and lower boundary conditions. Thus, it is not expected that  
310 a universal condition for all the significant droughts in the region can be identified. In fact, extreme  
311 drought events have been found in both El Nino and La Nina years. A previous study by Bonsal and  
312 Lawford (1999) indicates the meteorological drought often occurs after the mature phase of El Nino,  
313 which is not the case for 2015. The associated changes in the North Pacific represented by NPM positive  
314 phase is consistent with their results. The direct linkage between ENSO and the summer precipitation in  
315 the Canadian Prairies is not clear. In fact, the correlation between MEI and precipitation in the  
316 investigated region is -0.096 (p=0.239, sample size = 152). The region's growing season precipitation  
317 does not possess a significant correlation with ENSO, which is consistent with other researchers'  
318 findings (Dai and Wigley 2000).

319 The regression pattern is consistent with stationary Rossby wave theory as shown in a hierarchy  
320 of theoretical and modeling studies (Karoly *et al.* 1989, Simmons *et al.* 1983, Hoskins and Ambrizzi  
321 1993, Ambrizzi and Hoskins 1997, Held *et al.* 2002). A similar wave train extends from the western  
322 Pacific toward extra-tropical South America but at lower latitudes compared to its counterpart in the  
323 Northern Hemisphere (not shown). The node of the wave train in Western Canada and Northwest  
324 Pacific of the US corresponds to an anomalous ridge, which is in-phase of El Nino forcing. When the  
325 convection in the region associated with MJO-4 is weaker than normal (MJO-4  $\geq 0$ ), a wave train with  
326 the opposite sign will reach western Canada which then counteracts the El Nino forcing. Thus, the weak  
327 correlation between Canadian Prairie precipitation and ENSO is understandable as MJO plays an  
328 additional role that enhances or cancels out the GPH anomaly caused by El Nino.

329 In mid-latitude North America, the atmospheric response to the tropical forcing in the western  
330 Pacific depends on the mean circulation condition associated with tropical SST. Intraseasonal tropical  
331 convection oscillation in the western Pacific associated with MJO-4 index cannot determine the sign of  
332 precipitation anomaly in the prairies alone. Both warm SST in central Pacific and strong tropical  
333 convection in western Pacific and Maritime Continent are essential to cause a significant precipitation  
334 deficit in the western Canadian Prairies. Warm SST in central Pacific causes an eastward expansion of  
335 Pacific warm pool that favours enhanced MJO activity in the western-central Pacific (Hendon *et al.*  
336 1999, Marshall *et al.* 2016). In the year 2015, the SST anomaly in the Pacific (e.g. ENSO, NPM) forced  
337 the anomalous ridge on the west coast of Canada. This positive GPH anomaly was associated with the  
338 strong negative MJO4 indices, it then caused a blocking pattern and suppressed precipitation in the  
339 Canadian Prairies in the early summer. Although the El Nino continued to strengthen in July and August  
340 2015, the active convection associated with MJO in the western Pacific propagated eastward into the  
341 central Pacific. As the convection in the western Pacific/Maritime Continent waned, the precipitation in  
342 the Canadian Prairie returned to slightly above normal in July.

343 Fig. 8 The regression of stream function, wind field in the extratropics on MJO-4 for May-August with MEI  $\geq 0.5$ .  
344 Bottom: OLR, velocity potential, and divergent wind in the tropics on MJO-4 indices for May-August with  
345 NINO4 $>0.5$ . The shaded region for the tropical OLR has p-value  $\leq 0.05$ . Blue shading indicates active convection region.  
346 Red dashed contour and solid blue contour corresponds to negative and positive velocity potential, respectively.

347

## 348 5 Conclusions

349 The cause of the 2015 summer precipitation deficit in the western Canadian Prairies is  
350 investigated in relation to atmospheric circulation anomalies, SST, and intraseasonal tropical convection  
351 oscillation, MJO. The drought in western Canada is immediately related to an anomalous upper-level

352 ridge that persisted over the west coast of Canada and Alaska since fall 2014. This ridge was likely  
353 associated with a developing El Nino that was enhanced by the MJO.

354 In general, MJO-4 indices demonstrated significant correlation with the meteorological drought  
355 happened over west Canadian Prairies from May to August when warm SST presented in central Pacific  
356 ( $\text{NINO}_4 > 0$ ) with strong MJO amplitude. Our study discovered that MJO phase/strength is connected to  
357 the anomalous ridge over western Canada through the propagation of stationary Rossby wave from the  
358 western Pacific when  $\text{NINO}_4$  is positive. Though seasonally MJO is weaker in summer, the spring and  
359 early summer MJO amplitude is larger than normal when the central Pacific SST is warmer than normal  
360 ( $\text{NINO}_4 > 0$ ). The teleconnection between the Canadian Prairie precipitation deficit and MJO is stronger  
361 when  $\text{NINO}_4$  is positive. The underlying cause of this significant correlation between MJO-4 indices  
362 and the prairie precipitation in May-August is a stationary Rossby wave train originating from the  
363 Maritime Continent and western Pacific which propagates into Canada. The raytracing experiments  
364 show the main difference between a warm phase of  $\text{NINO}_4$  and a cold phase is the changes in stationary  
365 Rossby wave wavenumber over the source region. Under  $\text{NINO}_4 > 0.5$  May-August condition, the total  
366 wavenumber is about 4 and can propagate into western Canada if they oriented relatively zonally.  
367 Compared to  $\text{NINO}_4 > 0.5$ ,  $\text{NINO}_4 < -0.5$  corresponds to a weaker zonal wind and stronger meridional  
368 gradient of absolute vorticity in the subtropics of the source region (140-150E), hence the wavenumbers  
369 of stationary Rossby waves from the source region are larger (about 6), and fail to reach the Western  
370 Hemisphere. The intra-seasonal predictability of the growing season precipitation in the Canadian  
371 Prairies can be potentially improved by including the MJO amplitude and phase factors for medium-  
372 range/intra-seasonal projection in addition to ENSO effect especially when the central-Pacific SST is  
373 warm.

374

375 **Acknowledgement**

376 We gratefully acknowledge the Natural Sciences and Engineering Research Council of Canada  
377 (NSERC) for funding the Changing Cold Regions Network (CCRN) through their Climate Change and  
378 Atmospheric Research (CCAR) Initiative. Dr. Zhenhua Li is supported by the Probing the Atmosphere  
379 of the High Arctic project sponsored by the NSERC. Dr. Yanping Li gratefully acknowledges the  
380 support from the Global Institute of Water Security at the University of Saskatchewan. This research is  
381 also supported by Environment and Climate Change Canada (ECCC).

382 **References**

383 Ambrizzi T and Hoskins B J 1997: Stationary Rossby-Wave Propagation in a Baroclinic Atmosphere,  
384 *Quart. J. Roy. Meteor. Soc.*, **123** 919–28.

385 Andrews, E.D., R.C. Antweiler, P.J. Neiman, and F.M. Ralph 2004 Influence of ENSO on Flood  
386 Frequency along the California Coast. *J. Climate*, **17**, 337–348, doi: 10.1175/1520-0442(2004)017.

387 Bonsal, B.R., Chakravarti, A.K. and Lawford, R.G. 1993: Teleconnections between North Pacific SST  
388 Anomalies and Growing Season Extended Dry Spells on the Canadian Prairies, *Int. J. Climatol.*, **13**,  
389 865-878.

390 Bonsal, B.R., Zhang, X. and Hogg, W.D., 1999: Canadian Prairie growing season precipitation  
391 variability and associated atmospheric circulation, *Climate Research*, **11**(3), 191-208.

392 Bonsal B and Lawford R 1999: Teleconnections between El Niño and La Niña Events and Summer  
393 Extended Dry Spells on the Canadian Prairies, *International Journal of Climatology*, **19**, 1445–58.

394 Bonsal B R, Shabbar A and Higuchi K, 2001: Impacts of Low Frequency Variability Modes on  
395 Canadian Winter Temperature, *Int. J. Climatol.* **21**, 95–108.

396 BONSAL, B.R. and E. WHEATON. 2005: Atmospheric circulation comparisons between the 2001  
397 and 2002 and the 1961 and 1988 Canadian Prairie droughts. *Atmosphere-Ocean*, 43 (2): 163–  
398 172.

399 Bonsal B R and Regier M, 2007: Historical Comparison of the 2001/2002 Drought in the Canadian  
400 Prairies, *Climate Research*, **33**, 229-242.

401 Bonsal, B R, Aider, R, Gachon, P and Lapp S, 2013: An Assessment of Canadian Prairie Drought: Past,  
402 Present, and Future, *Climate Dynamics*, **41**, 501–516.

403 Carbone R. E., Yanping Li, 2015: Tropical Oceanic Rainfall and Sea Surface Temperature Structure:  
404 Parsing Causation from Correlation in the MJO, *Journal of Atmospheric Science*, Vol. 72, No. 7, 2703–  
405 2718.

406 Cassou C, 2008: Intraseasonal Interaction Between the Madden-Julian Oscillation and the North  
407 Atlantic Oscillation, *Nature*, **455** 523–7.

408 Dai A and Wigley T M L, 2000: Global Patterns of ENSO-Induced Precipitation, *Geophys. Res. Lett.*,  
409 **27** 1283–6.

410 Dee D P, Uppala S M, Simmons A J, Berrisford P, Poli P, Kobayashi S, Andrae U, Balmaseda M A,  
411 Balsamo G, Bauer P, Bechtold P, Beljaars A C M, Berg L van de, Bidlot J, Bormann N, Delsol C,  
412 Dragani R, Fuentes M, Geer A J, Haimberger L, Healy S B, Hersbach H, Hólm E V, Isaksen L, Kållberg  
413 P, Köhler M, Matricardi M, McNally A P, Monge-Sanz B M, Morcrette J-J, Park B-K, Peubey C,  
414 Rosnay P de, Tavolato C, Thépaut J-N, and Vitart F, 2011: The ERA-Interim Reanalysis: Configuration  
415 and Performance of the Data Assimilation System, *Quarterly Journal of the Royal Meteorological  
416 Society*, **137**, 553–97.

417 Dey B, 1982: Nature and Possible Causes of Droughts on the Canadian Prairies-Case Studies, *Journal of  
418 Climatology*, **2**, 233–49.

419 Garfinkel C I, Feldstein S B, Waugh D W, Yoo C and Lee S, 2012: Observed Connection Between  
420 Stratospheric Sudden Warmings and the Madden-Julian Oscillation, *Geophys. Res. Lett.*, **39**.

421 Hanesiak, J. M., Stewart, R. E., Bonsal, B. R., Harder, P., Lawford, R., Aider, R., *et al.* (2011).

422 Characterization and Summary of the 1999–2005 Canadian Prairie Drought. *Atmosphere-Ocean*, **49**(4),  
423 421–452. <http://doi.org/10.1080/07055900.2011.626757>

424 Hartmann D L, 2015: Pacific Sea Surface Temperature and the Winter of 2014, *Geophys. Res. Lett.*, **42**,  
425 1894–902.

426 Held I. M., Ting M. and Wang H., 2002: Northern Winter Stationary Waves: Theory and Modeling *J.*  
427 *Climate*, **15**, 2125–44.

428 Hendon, H. H., C. Zhang, and J. D. Glick, 1999: Interannual variation of the Madden-Julian Oscillation  
429 during Austral summer, *J. Clim.*, **12**, 2538–2550

430 Hong, C. C., Hsu, H. H., Tseng, W.-L., Lee, M. Y., Chow, C.-H., & Jiang, L.-C. 2017: Extratropical  
431 Forcing Triggered the 2015 Madden–Julian Oscillation–El Niño Event. *Sci. Rep.* **7**, 46692; doi:  
432 [10.1038/srep46692](https://doi.org/10.1038/srep46692).  
Hoskins B J and Ambrizzi T, 1993: Rossby Wave Propagation on a Realistic  
433 Longitudinally Varying Flow. *J. Atmos. Sci.* **50** 1661–71

434 Hoskins, B.J. and D.J. Karoly, 1981: [The Steady Linear Response of a Spherical Atmosphere to](#)  
435 [Thermal and Orographic Forcing. \*J. Atmos. Sci.\*, \*\*38\*\*, 1179–1196,](#)[https://doi.org/10.1175/1520-0469\(1981\)038<1179:TSLROA>2.0.CO;2](https://doi.org/10.1175/1520-0469(1981)038<1179:TSLROA>2.0.CO;2)

437 Hoskins, B.J. and T. Ambrizzi, 1993: [Rossby Wave Propagation on a Realistic Longitudinally Varying](#)  
438 [Flow. \*J. Atmos. Sci.\*, \*\*50\*\*, 1661–1671,](#)[https://doi.org/10.1175/1520-0469\(1993\)050<1661:RWPOAR>2.0.CO;2](https://doi.org/10.1175/1520-0469(1993)050<1661:RWPOAR>2.0.CO;2)

440 Huang B, Banzon V F, Freeman E, Lawrimore J, Liu W, Peterson T C, Smith T M, Thorne P W,  
441 Woodruff S D and Zhang H-M, 2015: Extended Reconstructed Sea Surface Temperature Version 4  
442 (ERSST. v4). Part I: Upgrades and Intercomparisons *Journal of Climate*, **28**, 911–30.

443 Kalnay E, Kanamitsu M, Kistler R, Collins W, Deaven D, Gandin L, Iredell M, Saha S, White G,

444 Woollen J, Zhu Y, Chelliah M, Ebisuzaki W, Higgins W, Janowiak J, Mo K, Ropelewski C, Wang J,

445 Leetmaa A, Reynolds R, Jenne R and Joseph D, 1996: The NCEP/NCAR 40-Year Reanalysis Project

446 *Bull. Amer. Meteor. Soc.* **77** 437–71

447 Karoly D J, Plumb R A, and Ting M, 1989: Examples of the Horizontal Propagation of Quasi-Stationary

448 Waves. *J. Atmos. Sci.* **46** 2802–11

449 Lee M Y, Hong C C and Hsu H H 2015: Compounding Effects of Warm Sea Surface Temperature and

450 Reduced Sea Ice on the Extreme Circulation Over the Extratropical North Pacific and North America

451 During the 20132014 Boreal winter *Geophys. Res. Lett.*, **42**, 1612–8.

452 Li Y., Richard E. Carbone, 2012: Excitation of rainfall over the tropical western Pacific. *Journal of*

453 *Atmospheric Science*, Vol. 69, No. 10, 2983–2994.

454 Li Y., Kit Szeto, Ron Stewart, Julie Theriault, Liang Chen, Bob Kochtubajda, Anthony Liu, Sudesh

455 Boodoo, Ron Goodson, Curtis Mooney, Sopan Kurkute, 2017: The June 2013 Alberta Catastrophic

456 Flooding: Water vapor transport analysis by WRF simulation. *Journal of Hydrometeorology*, Vol. 18,

457 2057-2078.

458 Li Z., Alan Manson, Yanping Li, Chris Meek, 2017: Circulation Characteristics of Persistent Cold

459 Spells in Central-Eastern North America. *Journal of Met. Res.*, Vol. 31, 250-260.

460 Liu J, Stewart R E and Szeto K K, 2004: Moisture Transport and Other Hydrometeorological Features

461 Associated With the Severe 2000/01 Drought Over the Western and Central Canadian Prairies *Journal*

462 *Of Climate*, **17**, 305–19.

463 Liu A., C. Mooney, K. Szeto, J. M. Thériault, B. Kochtubajda, R.E. Stewart, S. Boodoo, R. Goodson, Y.

464 Li, J. Pomeroy, 2016: The June 2013 Alberta Catastrophic Flooding Event: Part 1 – Large scale features.

465 *Hydrological Process*, 2016, 30, 4899–4916

466 Lorenz, D.J. and D.L. Hartmann, 2006: The Effect of the MJO on the North American Monsoon. *J.*

467 *Climate*, **19**, 333–343, doi: 10.1175/JCLI3684.1.

468 Madden R A and Julian P R, 1971: Detection of a 40-50 Day Oscillation in the Zonal Wind in the  
469 Tropical Pacific, *J. Atmos. Sci.*, **28**, 702–8

470 Marshall, A. G., H. H. Hendon, and G. Wang, 2016: On the role of anomalous ocean surface  
471 temperatures for promoting the record Madden-Julian Oscillation in March 2015, *Geophys. Res. Lett.*,  
472 43,472–481.

473 Riddle E E, Stoner M B, Johnson N C, L'Heureux M L, Collins D C and Feldstein S B, 2013: The  
474 Impact of the MJO on Clusters of Wintertime Circulation Anomalies Over the North American region  
475 *Climate Dynamics*, **40**, 1749–66.

476 Rodney, M., Lin, H., & Derome, J. 2013: Subseasonal Prediction of Wintertime North American  
477 Surface Air Temperature during Strong MJO Events. *Monthly Weather Review*, **141**(8), 2897–2909.  
478 <http://doi.org/10.1175/MWR-D-12-00221.1>.

479 Ropelewski C F and Halpert M S 1986: North American Precipitation and Temperature Patterns  
480 Associated with the El Niño/Southern Oscillation (ENSO), *Monthly Weather Review*, **114**, 2352–62.

481 Shabbar, A., Bonsal, B. and Khandekar, M., 1997: Canadian precipitation patterns associated with the  
482 Southern Oscillation. *Journal of Climate* 10:3016-3027.

483 Shabbar A and Skinner W, 2004: Summer Drought Patterns in Canada and the Relationship to Global  
484 Sea Surface Temperatures, *Journal of Climate*, **17**, 2866–80.

485 Shabbar A, Bonsal B R and Szeto K, 2011: Atmospheric and Oceanic Variability Associated with  
486 Growing Season Droughts and Pluvials on the Canadian Prairies, *Atmosphere-Ocean*, **49**, 339–55.

487 Simmons A J, Wallace J M and Branstator G W, 1983: Barotropic Wave Propagation and Instability,  
488 and Atmospheric Teleconnection Patterns, *J. Atmos. Sci.*, **40**, 1363–92.

489 Szeto, K., X. Zhang, R.E. White, and J. Brimelow, 2016: The 2015 Extreme Drought in Western  
490 Canada. *Bull. Amer. Meteor. Soc.*, **97**, S42–S46, <https://doi.org/10.1175/BAMS-D-16-0147.1>.

491 Wang S Y, Hipps L, Gillies R R and Yoon J-H, 2014: Probable Causes of the Abnormal Ridge  
492 Accompanying the 2013-2014, California Drought: ENSO Precursor and Anthropogenic Warming  
493 footprint *Geophys. Res. Lett.*, **41** 3220–6.

494 Xie P and Arkin P A, 1997: Global Precipitation: A 17-year Monthly Analysis Based on Gauge  
495 Observations, Satellite Estimates, and Numerical Model Outputs. *Bulletin of the American  
496 Meteorological Society*, **78**, 2539–58.

497 Xue Y, Higgins W and Kousky V 2002: Influences of the Madden-Julian Oscillations on Temperature  
498 and Precipitation in North America during ENSO-neutral and Weak ENSO Winters, *Proc. workshop on  
499 prospects for improved forecasts of weather and short-term climate variability on subseasonal (2 week  
500 to 2 month) time scales.*

501 Wheaton, E, Wittrock V, Kulshreshtha S, Koshida G, Grant C, Chipanshi A, Bonsal BR, 2005: Lessons  
502 Learned from the Drought Years of 2001 and 2002: Synthesis Report. Agriculture and Agri-Food  
503 Canada, Saskatchewan Research Council Publ No. 11602–46E03, Saskatoon.

504 Wheeler, M. C., & Hendon, H. H., 2004: An all-season real-time multivariate MJO index: Development  
505 of an index for monitoring and prediction. *Monthly Weather Review*, **132**(8), 1917–1932.

506 Wolter, K., 1987: The Southern Oscillation in surface circulation and climate over the tropical  
507 Atlantic, Eastern Pacific, and Indian Oceans as captured by cluster analysis. *J. Climate Appl.  
508 Meteor.*, **26**, 540-558.

509 Wolter, K. and M.S. Timlin, 1993: Monitoring ENSO in COADS with a seasonally adjusted principal  
510 component index. *Proc. of the 17th Climate Diagnostics Workshop*, Norman, OK,  
511 NOAA/NMC/CAC, NSSL, Oklahoma Clim. Survey, CIMMS and the School of Meteor., Univ. of  
512 Oklahoma, 52-57.

513 Zhang C, 2005: Madden-Julian Oscillation *Reviews of Geophysics*, **43**.

514

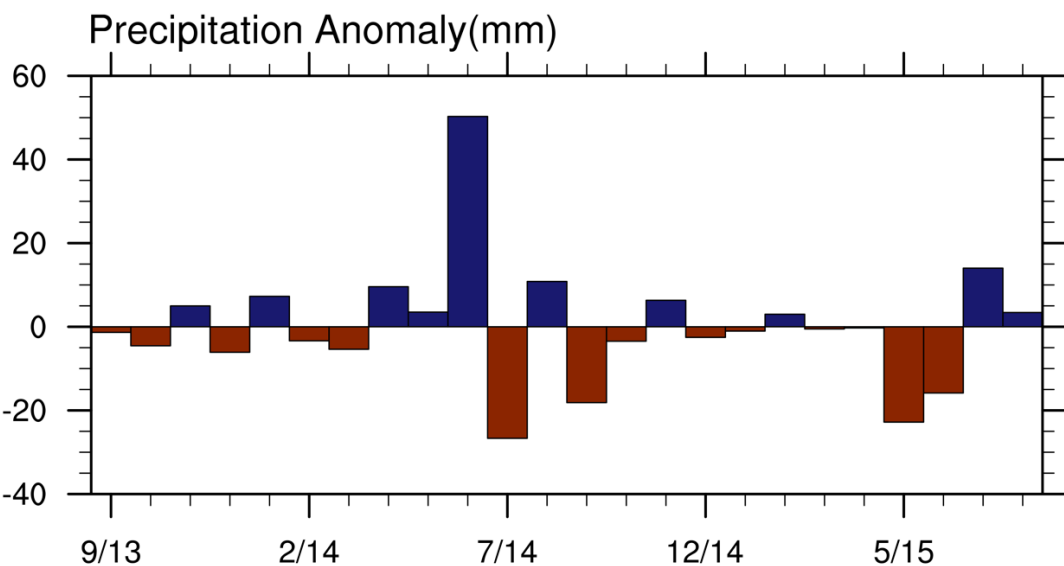
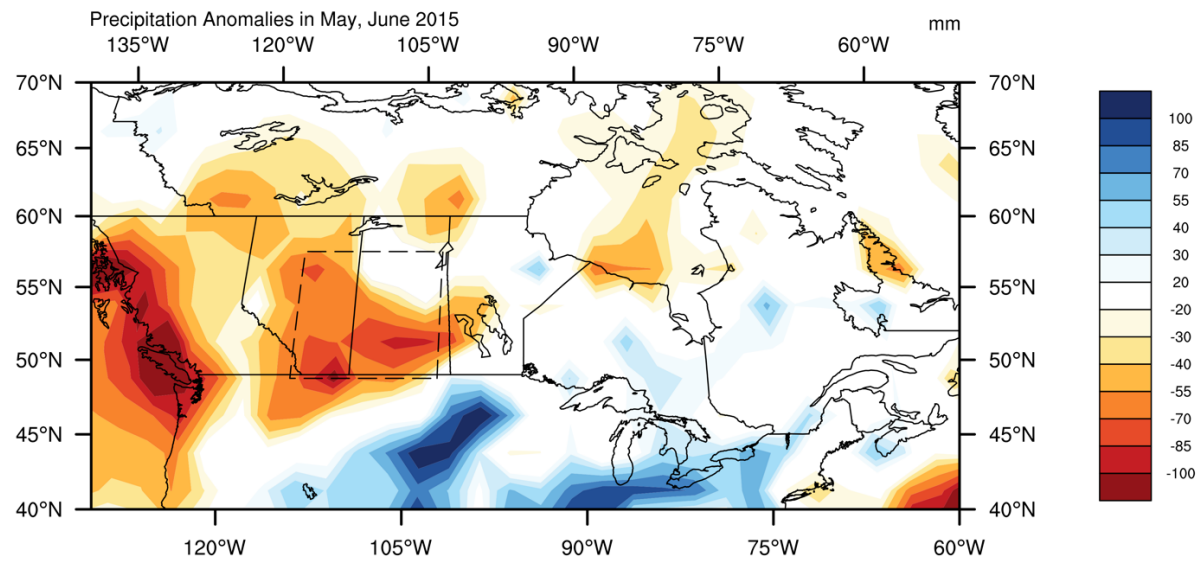
515

516

517 Table 1 Correlation between mean precipitation anomaly in the prairie from CMAP and MEI, MJO  
518 indices 4. MJO indices and CMAP are from 1979 to 2016.

	Correlation	p-value	No. of sample
MEI	-0.096	0.24	156
MJO-4	0.18	0.023	156
MJO-4(NINO4>0)	0.33	0.0015	90
MJO-4(NINO4<0)	-0.01	0.94	66

519



520

521 Fig. 1 Top: Precipitation anomalies (mm) from CMAP over the region (115 W-102.5 W, 50 N-57.5 N)  
 522 during May and June 2015. Bottom: time series of monthly precipitation anomaly over boxed region  
 523 between September 2013 and August 2015.

524

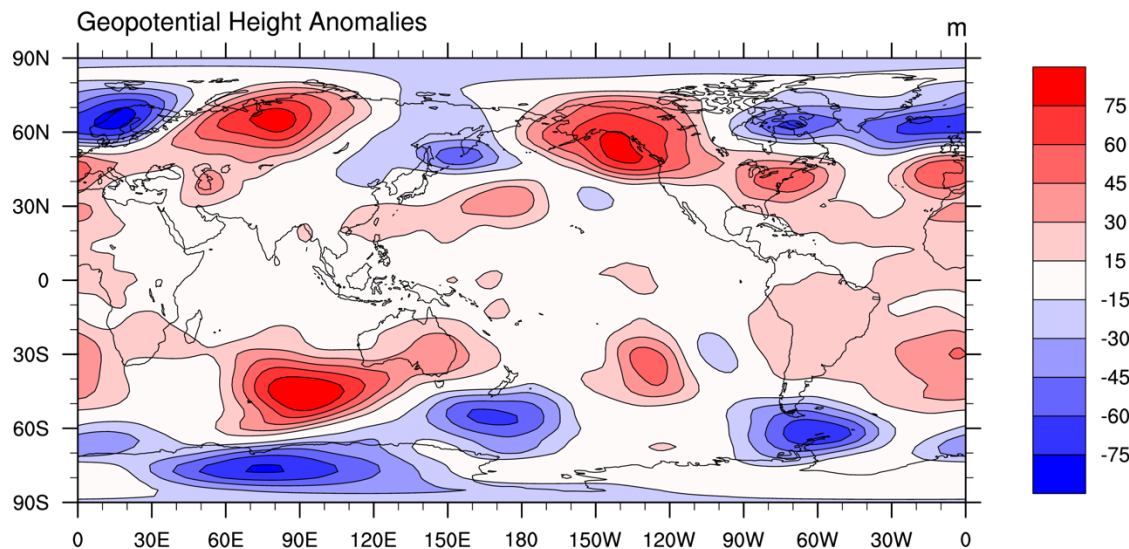
525

526

527

528

### Mean GPH Anomaly of May, June 2015



529

530 Fig. 2 NCEP GPH anomaly at 500hPa during May and June 2015 when the precipitation deficit was the  
531 largest.

532

533

534

535

536

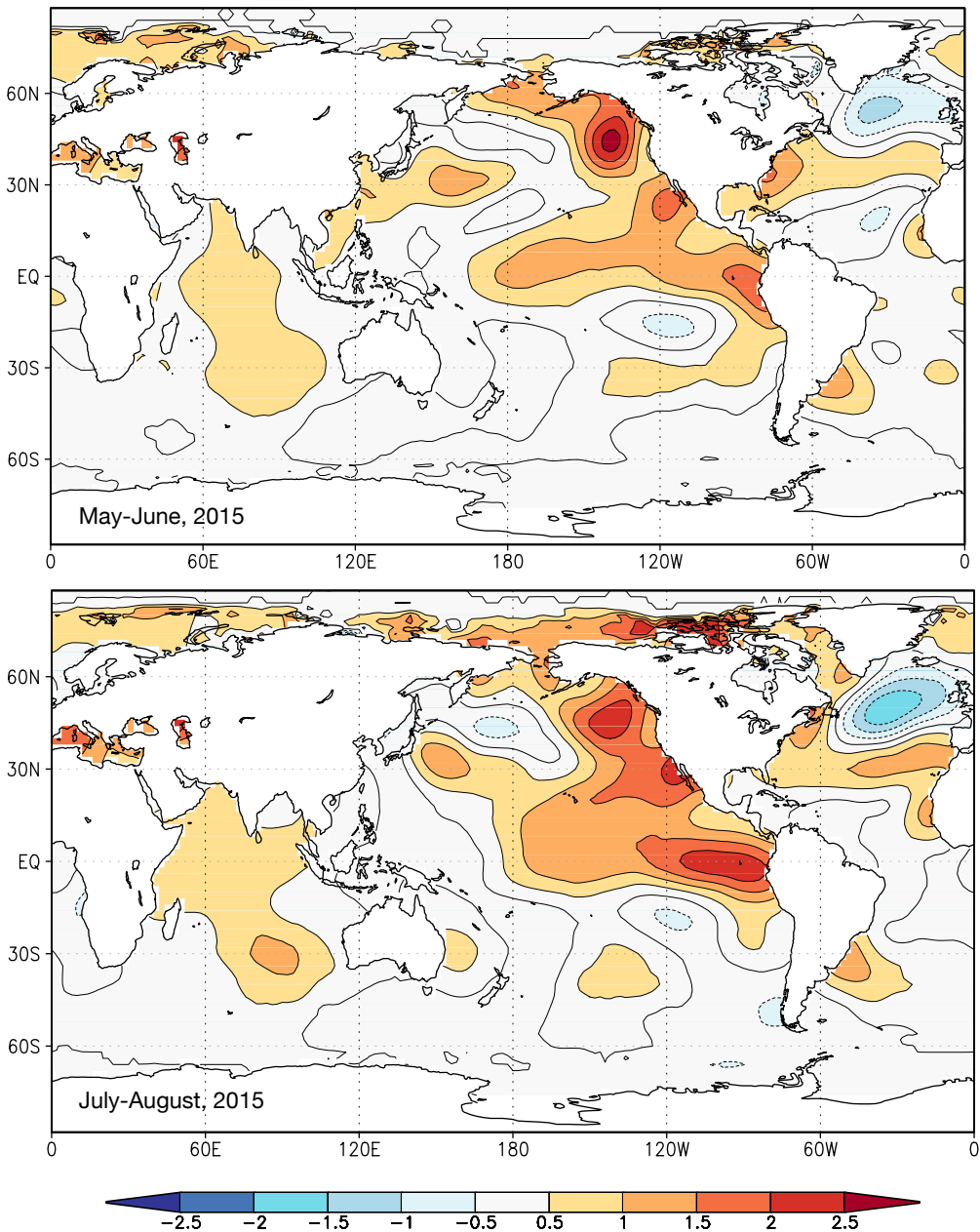
537

538

539

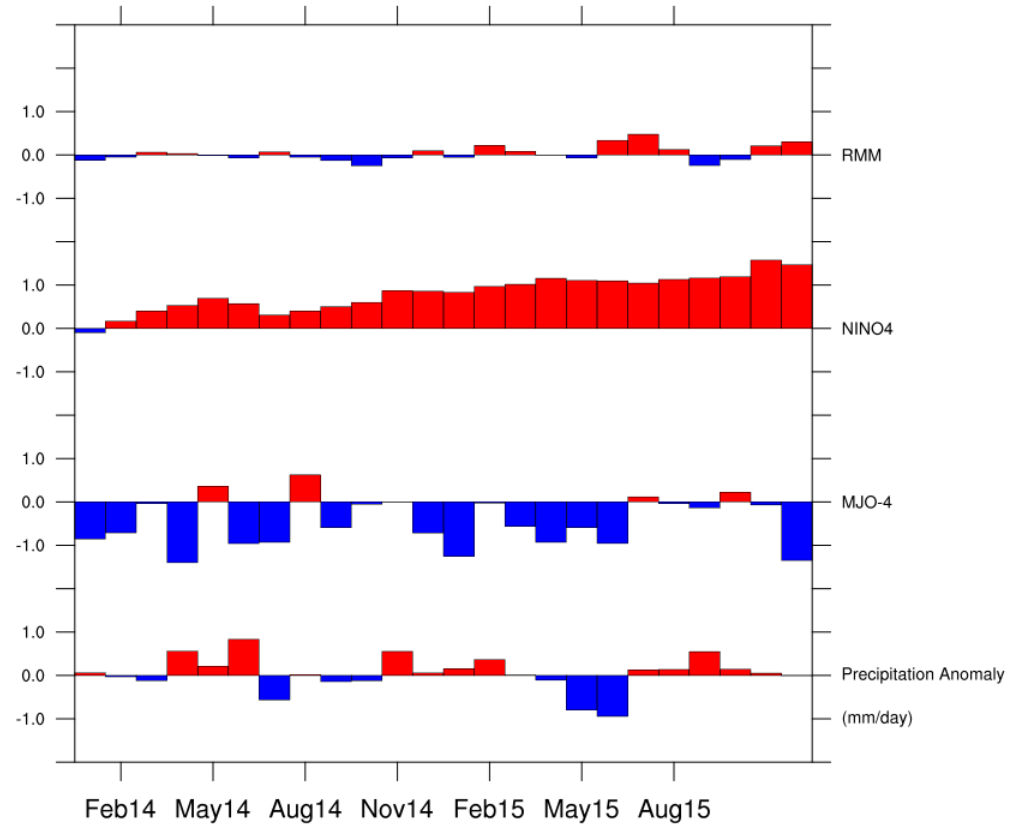
540

541



542

543 Fig. 3 The mean SST anomaly ( $^{\circ}\text{C}$ ) from ERSST v4 for May-June and July-August 2015.



544

545 Fig. 4 RMM amplitude anomaly, NINO4, MJO 4 indices and precipitation anomaly of Canadian Prairies  
 546 from January 2014 to Dec 2015.

547

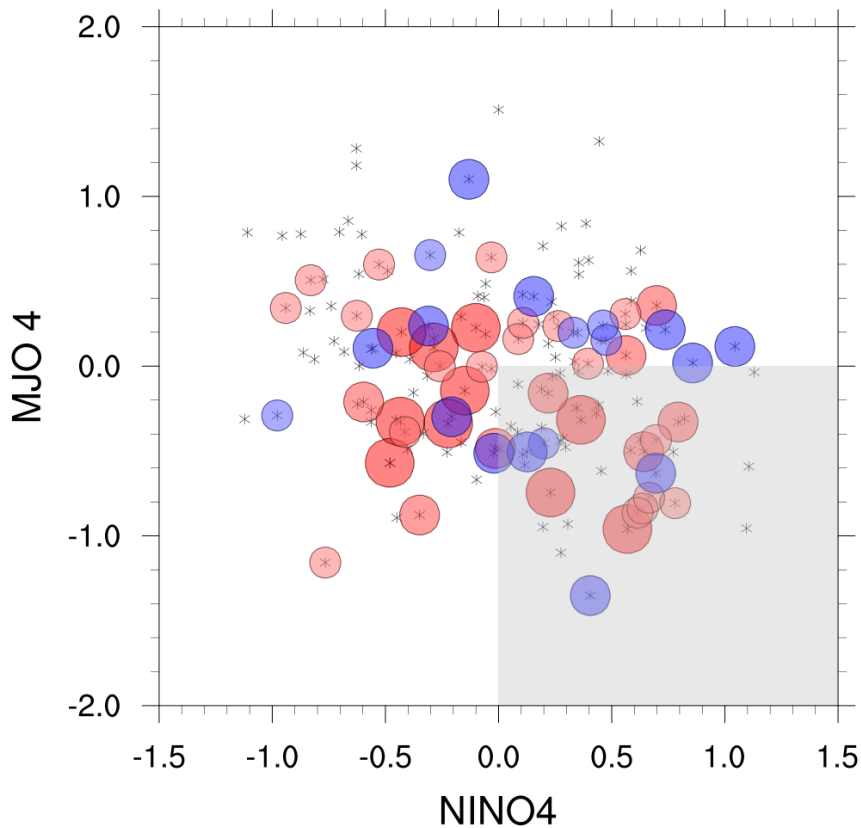
548

549

550

551

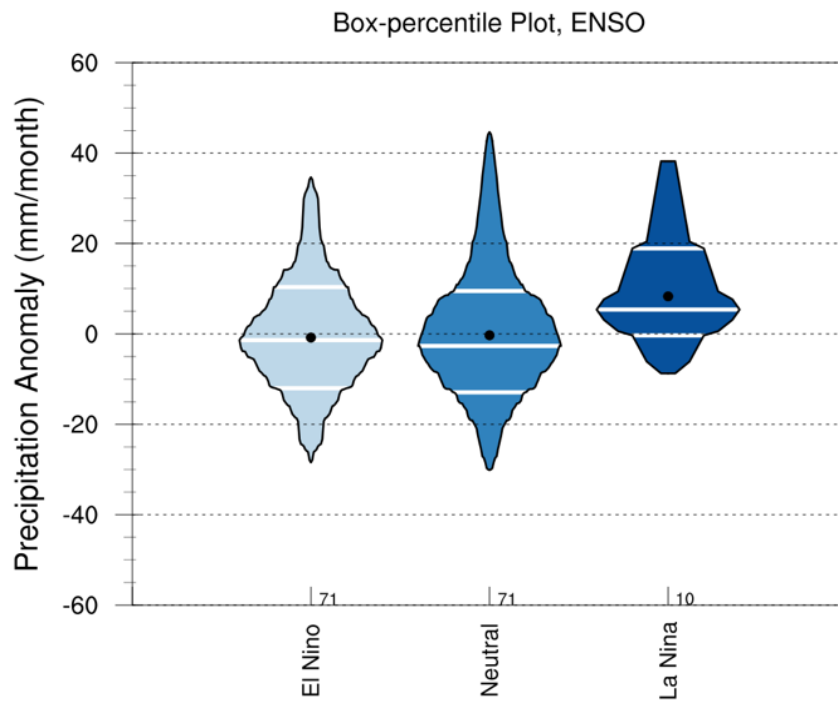
552



553

554 Fig. 5 The scatter plot of monthly precipitation anomaly (mm/month) as a function of MJO-4 and  
 555 NINO4. Each asterisk represents a month from May to August 1979-2016. Circled asterisk denotes a  
 556 month with precipitation anomaly larger than 18 mm/month. The blue circles are months with positive  
 557 precipitation anomaly and the red circles are months with negative precipitation anomaly. The sizes of  
 558 circles denote the magnitudes of the anomalies (large > 30 mm/month, medium > 24 mm/month,  
 559 small >18 mm/month). The shaded area denotes NINO4 > 0 and MJO-4 index < 0.

560



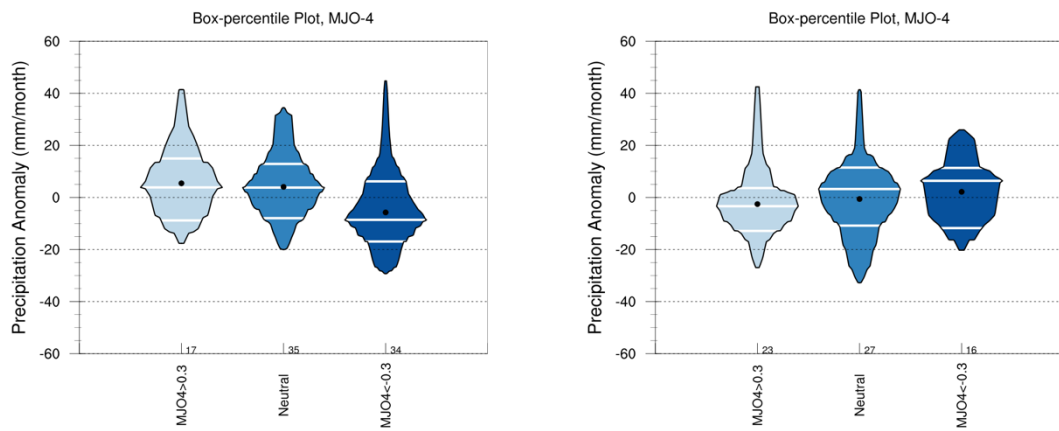
561

562 Fig. 6 The box-percentile plot of Canadian Prairies precipitation anomaly during growing season under  
563 different ENSO conditions.

564

565

566



567

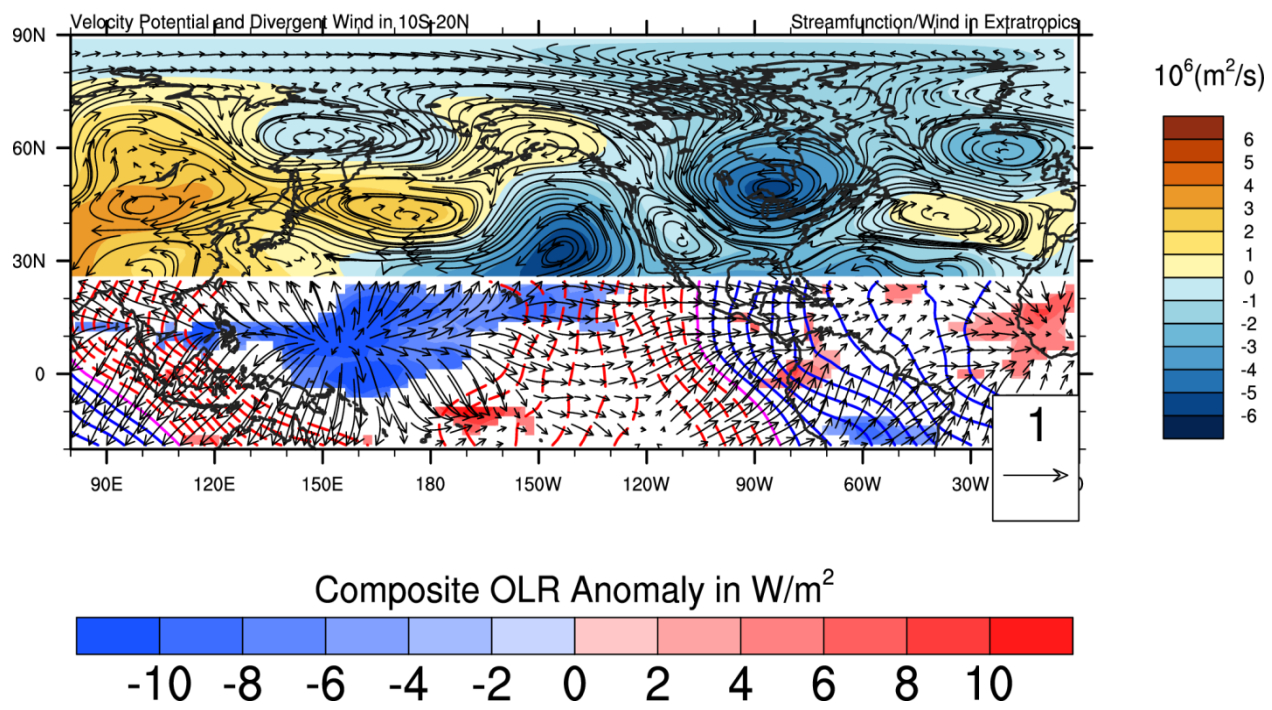
568

Fig. 7 Box-percentile plots of Canadian Prairies' precipitation anomaly during growing season

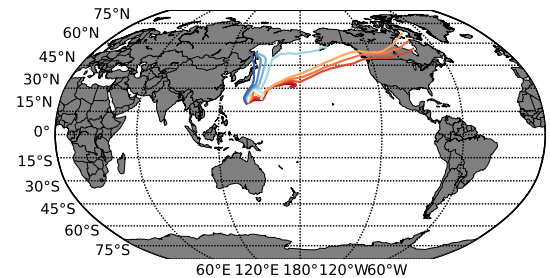
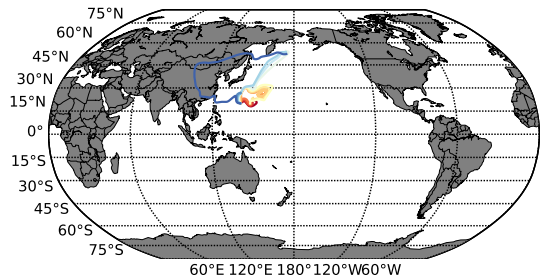
569

versus MJO-4 under warm NINO4 ( $\text{NINO4} > 0$ , left) and cold NINO4 ( $\text{NINO4} < 0$ , right) SST condition.

570



574 Fig. 8 The regression of stream function, wind field in the extratropics on MJO-4 for May-August with  
 575  $\text{NINO4} \geq 0.5$ . OLR, velocity potential, and divergent wind in the tropics on MJO-4 indices for May-  
 576 August with  $\text{NINO4} > 0.5$ . The shaded region for the tropical OLR has  $p$ -value  $\leq 0.05$ . Blue shading  
 577 indicates active convection region. Red dashed contour and solid blue contour corresponds to negative  
 578 and positive velocity potential, respectively.



582

583

584 *Fig. 9: Ray-tracing result with total wavenumber specified by the mean flow 140-150W and 20-30N for*  
 585 *mean May-August condition with  $\text{NINO4} < -0.5$  (left) and  $\text{NINO4} > 0.5$  (right). Rays originate from 140E,*  
 586 *20N with angles ranging from 0 (red) to 60 degree (dark blue) from zonal direction.*